Neural mechanisms of transient neocortical beta rhythms: Converging evidence from humans, computational modeling, monkeys, and mice

Maxwell A. Sherman[a,b], Shane Lee[a], Robert Law[a], Saskia Haegens[c,d], Catherine A. Thorn[a], Matti S. Hämäläinen[e,f,g], Christopher I. Moore[a], and Stephanie R. Jones[a,1]

[a]Department of Neuroscience, Brown University, Providence, RI 02912; [b]Department of Applied Mathematics, Brown University, Providence, RI 02912; [c]Cognitive Neuroscience and Schizophrenia Program, Nathan Kline Institute, Orangeburg, NY 10962; [d]Department of Neurological Surgery, College of Physicians and Surgeons, Columbia University, New York, NY 10032; [e]Athinola A. Martinos Center, Massachusetts General Hospital, Boston, MA 02129; [f]Department of Neuroscience and Biomedical Engineering, Aalto University School of Science, 02150 Espoo, Finland; and [g]Harvard Medical School, Boston, MA 02115

Edited by Nancy Kopell, Boston University, Boston, MA, and approved June 21, 2016 (received for review March 28, 2016)

Human neocortical 15–29-Hz beta oscillations are strong predictors of perceptual and motor performance. However, the mechanistic origin of beta in vivo is unknown, hindering understanding of its functional role. Combining human magnetoencephalography (MEG), computational modeling, and laminar recordings in animals, we present a new theory that accounts for the origin of spontaneous neocortical beta. In our MEG data, spontaneous beta activity from somatosensory and frontal cortex emerged as noncontinuous beta events typically lasting <150 ms with a stereotypical waveform. Computational modeling uniquely designed to infer the electrical currents underlying these signals showed that beta events could emerge from the integration of nearly synchronous bursts of excitatory synaptic drive targeting proximal and distal dendrites of pyramidal neurons, where the defining feature of a beta event was a strong distal drive that lasted one beta period (~50 ms). This beta mechanism rigorously accounted for the beta event profiles; several other mechanisms did not. The spatial location of synaptic drive in the model to supragranular and infragranular layers was critical to the emergence of beta events and led to the prediction that beta events should be associated with a specific laminar current profile. Laminar recordings in somatosensory neocortex from anesthetized mice and awake monkeys supported these predictions, suggesting this beta mechanism is conserved across species and recording modalities. These findings make several predictions about optimal states for perceptual and motor performance and guide causal interventions to modulate beta for optimal function.

beta rhythm | magnetoencephalography | computational modeling | sensorimotor processing | Parkinson's disease

Beta band rhythms (15–29 Hz) are a commonly observed activity pattern in the brain. They are found with magnetoencephalography (MEG) (1–4), EEG (5, 6), and local field potential (LFP) recordings from neocortex (7–9) and are preserved across species (10). Local beta oscillations and their coordination between regions are implicated in numerous functions, including sensory perception, selective attention, and motor planning and initiation (2, 3, 6, 7, 9, 11–15). Neocortical beta oscillations are disrupted in various neuropathologies, most notably Parkinson's disease (PD), in which treatments that alleviate motor symptoms also reverse the neocortical beta disruption (16, 17). Although associations between beta and performance suggest a crucial role in brain function, beta rhythmicity might not be important per se but instead may be an epiphenomenal consequence of other important processes. Discovering how beta emerges at the cellular and network levels is crucial to understanding why beta is such a clear predictor of performance in many domains.

A major, unresolved point of debate concerns the locus of beta generation. One prominent view is that beta is generated in basal ganglia and thalamic structures and that neocortical beta is an entrained reflection of these inputs. Alternatively, beta may emerge within the neocortex as a consequence of internal dynamics. An intermediate view, supported by the model presented here, is that beta emerges in the neocortex but is dependent on extrinsic synaptic drive that could originate from basal ganglia/thalamus. Consistent with the first view, beta has been robustly observed in LFP signals from basal ganglia nuclei including the subthalamic nucleus, striatum, and globus pallidus (18, 19), and computational models have proposed mechanisms by which beta rhythms can emerge via interactions within and between these circuits (20, 21). Other studies have suggested that the neocortex itself has unique properties that generate beta rhythms through spike-mediated synaptic and electrical interactions within local circuits (22–25) or that beta in early-sensory neocortical areas could be driven in a top-down manner from frontal cortex during attentive states (26).

Understanding the temporal and spectral nature of a specific beta signal is critical to uncovering its mechanism of generation and its role in the precise local circuit and context in which it is observed. A common view of beta "rhythms" is that they are sustained in time for many cycles, up to seconds in duration. The view of beta as a sustained rhythm is consistent with several papers that have reported what appears to be a continuous, high-power increase in beta activity, for example during a planning or

Significance

Neocortical beta is one of the most prominent signatures of neural activity measured noninvasively in humans. Beta expression is a strong predictor of healthy and pathological perceptual and motor performance. However, there is considerable debate as to whether beta itself is causally important in information and disease processes. Key to resolving this debate is understanding the neural mechanisms inducing beta. Here, building on prior work, we combined human magnetoencephalography, computational modeling, and laminar recordings in mice and monkeys to establish and test a new theory explaining the emergence of spontaneous transient neocortical beta events in somatosensory and frontal cortex. Our results enable a principled understanding of neocortical beta and can help guide studies seeking to understand its relation to function.

Author contributions: M.A.S., S.L., C.I.M., and S.R.J. designed research; M.A.S., S.L., R.L., S.H., and C.A.T. performed research; M.A.S., S.L., and M.S.H. contributed new reagents/analytic tools; M.A.S., R.L., and S.H. analyzed data; and M.A.S., S.L., C.I.M., and S.R.J. wrote the paper.

The authors declare no conflict of interest.

This article is a PNAS Direct Submission.

Freely available online through the PNAS open access option.

[1]To whom correspondence should be addressed. Email: stephanie_jones@brown.edu.

This article contains supporting information online at www.pnas.org/lookup/suppl/doi:10.1073/pnas.1604135113/-/DCSupplemental.

"hold" period in a motor task or during the allocation of attention in sensory neocortices (2, 27–29). Data showing such effects are almost always averaged spectrograms or averaged power spectral density measurements taken from many individual trials aligned to functionally relevant events. However, burst-like or intermittent periods of high beta power occurring stochastically within the time-averaged period could appear as continuous rhythms in averaged spectrograms, despite not ever actually being sustained. Several recent studies have shown that in nonaveraged data beta oscillations often emerge transiently, typically lasting <150 ms (2, 4, 30–32).

Here, we combined human MEG, computational neural modeling, and laminar recordings in animals to propose a new theory to explain the origin of spontaneous beta activity that emerges transiently and intermittently in the awake mammalian neocortex. Building on our prior work (1, 2, 15, 33), we studied MEG-measured spontaneous beta activity in two brain areas: (*i*) primary somatosensory neocortex (SI), where beta emerges as part of the so-called "mu rhythm" and typically contains a complex of alpha and beta events, and (*ii*) frontal cortex, specifically the right inferior frontal cortex (IFC), where beta can be expressed without a strong alpha signal. We previously have shown that beta activity in each of these areas is coordinated, with synchrony in the beta band increasing during inattention (15) and increased beta power in SI predicting failed detection (2).

To uncover the neural mechanisms specific to beta generation, we first quantified beta's manifestation on individual trials. We verified that beta events in each area were independent of alpha events and were transient in time. Further, we found beta events had a consistent temporal profile. To study the cellular and network level mechanisms creating this beta activity, we used a biophysically principled model of a laminar cortical circuit designed specifically to simulate human MEG/EEG-measured primary current source signals (1, 34–37). In keeping the output of our model in close agreement with our MEG data, we arrived at the prediction that these beta events are not inherited linearly from subcortical structures or generated by the spiking interactions in local neocortical circuits. Rather, our data suggest that transient beta events emerge locally in neocortex from the integration of synchronous bursts of subthreshold excitatory synaptic drive that simultaneously target both proximal and distal dendrites of pyramidal neurons (PNs), such that the distal input is sufficiently strong and lasts a beta period.

Our beta theory predicted a specific neocortical laminar current profile during beta events that was supported by laminar recordings in mice and monkeys. In sum, our model accurately reproduces beta events found in SI and in higher-order frontal area IFC and accurately reflects the data generated in distinct species, in distinct recording modalities (MEG and invasive laminar electrophysiological recordings), and in distinct brain states (anesthetized versus awake-behaving).

Results

Human Neocortical Beta Occurs as Stereotypical Brief Events. We studied source-localized human MEG data from the hand area of SI and from IFC. These signals were investigated in prior studies (1, 15), where we applied inverse modeling techniques to estimate the location, magnitude, and temporal evolution of spontaneous activity. Here, we investigated the signatures of spontaneous beta activity in the prestimulus period in each of these signals (*Experimental Procedures*, *MEG Data*). Examples of the spontaneous activity and corresponding time–frequency spectrogram in nonaveraged and averaged data in each area are shown in Fig. 1*A*. In nonaveraged data, beta shows brief periods of high power falling off sharply to background activity levels. To characterize these beta events, we analyzed 50 events with the highest peak power from each dataset (*SI Appendix*, *Experimental Procedures*, *Defining High-Power Beta Events*). The duration of these beta events was quantified as the time that beta power was above a certain threshold. To determine a principled threshold for high-power beta events, we created an empirical distribution of beta power across all trials and time. We chose the 98th percentile of this power distribution as the threshold, because this cutoff was below the maximum power of all high-power beta events used in further analyses. Using this threshold, we found that the duration of events typically lasted approximately three periods (e.g., ~150 ms) (*SI Appendix*, *Experimental Procedures* and Tables S1 and S2). Continuous bands of beta activity appeared only when the spectrograms were averaged across many trials (mean $n = 100$) (Fig. 1*A*, *Bottom*; also see refs. 1 and 30). In SI, beta activity typically co-occurred with strong alpha events but could emerge with very little alpha (Fig. 1*A*; see also ref. 33). In IFC beta also occurred with varying levels of alpha activity (Fig. 1*A*). The peak frequency of the beta events in IFC (20–27 Hz) (*SI Appendix*, Table S2) was typically higher than in SI (18–22 Hz) (*SI Appendix*, Table S1). However, when measured in the spectral domain, the duration of the high-power beta events was approximately three beta periods in each area (SI: 3.37 ± 0.12; IFC: 3.15 ± 0.13) (*SI Appendix*, Tables S1 and S2).

The raw current source waveforms (red boxes in Fig. 1*A*) suggested that high-power beta events had a stereotypical waveform so that the polarity and temporal profile were highly consistent within and across subjects and exhibited a large negative deflection. The average of 50 high-power beta events in SI and IFC from example subjects, aligned to the maximum extrema in the waveform that was closest to the time of greatest spectral power in the corresponding spectral beta event (*SI Appendix*, *Experimental Procedures*, *Aligning Peaks*), showed that the waveform was not sinusoidal. Rather, the beta event contained a dominant trough that was preserved across events in each subject and in the average across subjects in each area (SI: $n = 10$ subjects; IFC: $n = 9$ subjects; see the dominant negative amplitude trough labeled PK3 in Fig. 1*B*). Although the amplitude of the peaks in the aligned waveforms varied across subjects and areas, the temporal profiles were consistent and symmetric around the large-amplitude PK3 trough, suggesting that a highly stereotypical underlying biophysical process may create this trough activity.

Several key features defining the shape of the beta event waveforms were statistically significant within and across subjects in both SI and IFC. These features are shown schematically in the lower panels in Fig. 1 *B*, *i* and *iii* and are quantified in *SI Appendix*, *Experimental Procedures*, *Quantification of Beta Events* and Tables S1 and S2. The amplitude of the PK3 was opposite in sign to the neighboring PK2 and PK4 peaks (PK3: negative; PK2 and PK4: positive) and was larger in absolute magnitude than the PK1 and PK5 peaks. The PK3 trough was also the sharpest peak in both SI and IFC, i.e., the slopes from PK2 to PK3 and from PK3 to PK4 were steeper than those between other peaks. In SI, the PK3 was larger in absolute magnitude than the PK2 and PK4 peak in most (9/10) subjects. However this feature was inconsistently observed in IFC signal (2/9 subjects). Further, in IFC, the averaged beta event from each subject had clear negative PK1 and PK5 troughs (Fig. 1 *B*, *iv*) that were not consistently negative in the SI averages (Fig. 1 *B*, *ii*) and were not consistently observed in all individual high-power beta events in SI or IFC (e.g., Fig. 1 *B*, *i* and *iii*).

The duration of the dominant PK3 trough determined the frequency of the beta event. The PK3 duration was a better predictor of the beta period than the duration of other interpeak intervals in both SI and IFC (Pearson's correlation $P < 0.01$) (*SI Appendix*, Table S3). PK3 duration is defined as the time between PK2 and PK4 extrema for each event (see mean duration, *SI Appendix*, Tables S1 and S2). This observation implies that the duration of the PK3 trough plays a dominant role in determining the frequency of the beta event, and its larger magnitude implies that the amplitude of the PK3 trough largely determines the power of the event.

In summary, the statistically significant features of the beta waveforms within and across subjects, and conserved across areas, were contained around the dominant trough, a region from the

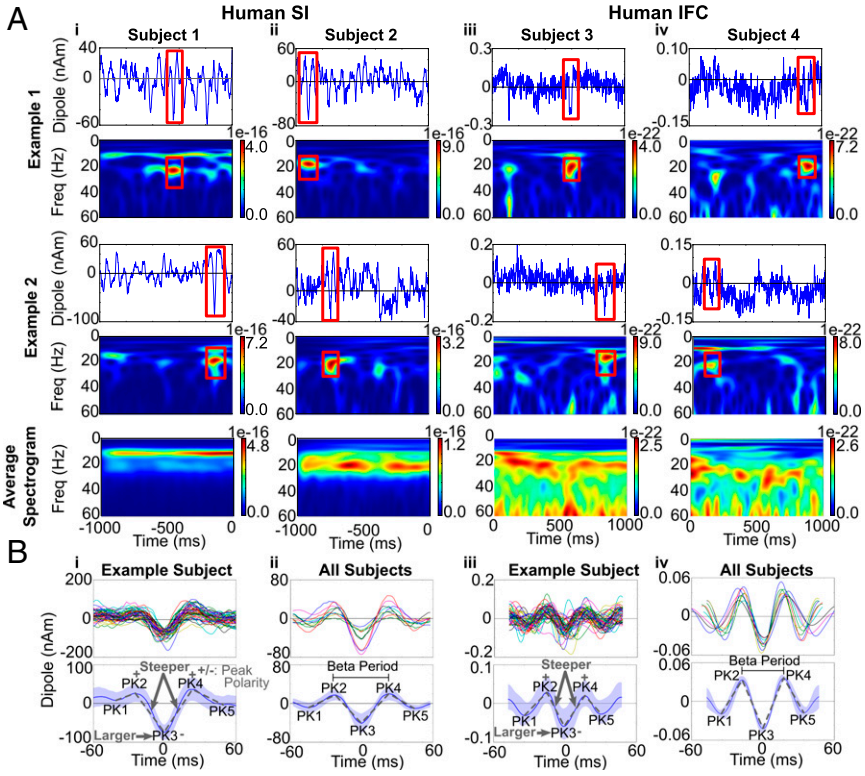

Fig. 1. Spontaneous rhythms in human SI and IFC current source signals show transient beta events with a stereotypical shape. (*A*) Examples of spontaneous oscillations and corresponding time–frequency spectrograms over 1-s epochs observed in MEG source-localized data from SI and IFC in four different subjects [units: $(AM)^2$]. In nonaveraged data beta oscillations (red boxes) emerged transiently, with high-power beta events lasting approximately three periods (*SI Appendix*, Tables S1 and S2). (*Bottom Row*) Continuous oscillations) appear only when data are averaged over many 1-s cycles (n = 100 1-s epochs). (*B*, *i*) Temporal profile of 50 high-power beta events in SI from a sample subject aligned to the trough closest to the time of maximum power of the corresponding spectral beta event (*Upper*) and corresponding average and SD (*Lower*). (*ii*) Average of 50 high-power beta events in 10 different subjects (*Upper*) and corresponding average and SD (*Lower*). (*iii* and *iv*) Analogous results for IFC. In each area, the beta event waveforms had a stereotypical shape with quantifiable features, depicted schematically in the lower panels (see text and *SI Appendix*, Tables S1 and S2).

points labeled PK1 to PK5 that resembled an inverted Ricker wavelet (Fig. 1*B*). This shape was sufficient to create high-power beta events in nonaveraged data (e.g., Fig. 1 *B*, *i*; see also Fig. 8 and *SI Appendix*, Fig. S2), and the duration of the PK3 determined the beta frequency of the beta event. Below we address how our computational model can account for these statistically significant features and discuss parameters that can generate additional waveform attributes as well as differences in beta events across individual events, subjects, and areas.

Detailed Neocortical Modeling Provides a Specific Explanation for Human Current Source Signals. Key to the development of our theory of beta emergence was construction of a computational model of a laminar neocortical circuit uniquely designed to reproduce the primary electrical currents underlying macroscopic MEG/EEG signals accurately (1, 34–37). The neural origin of the estimated primary currents (J^p) is thought to be the aggregate of postsynaptic longitudinal currents flowing inside the apical dendrites of the large, spatially aligned neocortical PNs (Fig. 2) (35–39).

Crucially, the model contained multi-compartment PNs in supra- and infragranular layers. The primary current signals were simulated as the net intracellular current flow in a direction parallel to the long apical dendrites, with units directly comparable to the MEG data (expressed as current (nA) × distance (m), or nanoampere meters, nAm) (1, 34–37). The PNs were embedded in a laminar model of a neocortical column (100 PNs, 35 interneurons per layer) that received an AMPAergic excitatory postsynaptic drive to the granular and supragranular layers (Fig. 3 *B*–*D*). These exogenous drives, potentially arising from thalamic or higher-order neocortical areas, effectively drove postsynaptic excitatory currents through the proximal and distal dendrites of the PNs, producing alternating current flow in the simulated current source signal analogous to the current flow measured with MEG. We thus were able to test several theories of beta generation by directly comparing model output to MEG-measured beta events.

We tested several models based on specific hypotheses regarding the origin of neocortical beta rhythms. In each case, we compared the modeled output with the human data to see which mechanisms could accurately account for statistically robust features of the beta event waveforms. Specifically, our criteria for an accurate model of these beta events included reproduction of the large amplitude and beta period duration (~50 ms) of the PK3 trough; the steeper slopes of the PK3 trough compared with neighboring peaks; and the opposite sign of PK3 amplitude compared with PK2 and PK4. We show below that a refinement of our prior SI mu model could reproduce these statistically significant beta event waveform features accurately, but several alternative models of beta rhythmicity did not (*SI Appendix*, Table S5). Our model could also explain differences in the beta events between areas and subjects.

Our biophysically principled computational model predicts that beta events emerge from a weak and broad proximal drive simultaneous with a strong distal drive that lasts a beta period. Motivated by our prior study and experimental results presented here, we investigated more closely

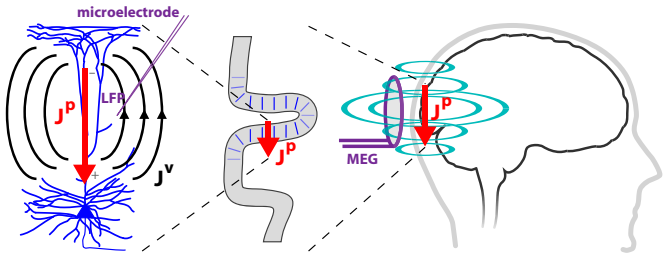

Fig. 2. Schematic illustration of the relationship between MEG primary current source signals and LFP. Inverse solution techniques applied to MEG (or EEG) sensor data estimate the location and magnitude of the primary electrical current sources (J^p) producing the recorded fields. These current sources are associated with the net postsynaptic currents flowing within the long, spatially aligned apical dendrites of large populations of PNs, enabling an interpretation of polarity in terms of the directionality of current flow within the PN dendrites (35, 37–39). The primary sources will also produce volume currents (J^v) and an associated extracellular potential distribution that can be recorded with microelectrodes as LFPs.

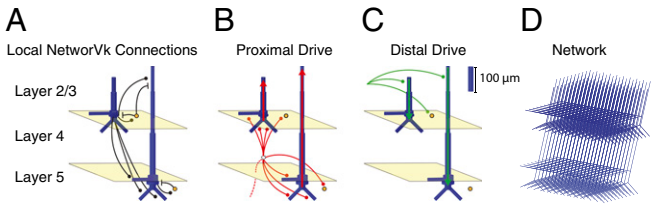

Fig. 3. Schematic of the laminar neocortical model used to simulate human MEG current source signal. (*A*) The model consisted of multi-compartment PNs (blue) in the supragranular (layers 2/3) and infragranular (layer 5) layers synaptically coupled to single-compartment inhibitory neurons (IN, orange) with AMPA (circles) and $GABA_A$ (lines) synapses. (*B*) The proximal drive is an excitatory synaptic drive presumed to come from lemniscal thalamus that is propagated through the granular layer (layer 4) and effectively contacts the proximal dendrites of the PN and the INs. (*C*) the distal drive is an excitatory synaptic drive presumed to come from nonlemniscal thalamus that contacts the PN distal dendrites and INs in the supragranular layers. (*D*) The network contained 100 PNs and 35 INs per layer. The simulated SI current dipole signal was calculated as net intracellular current flow in the PN dendrites in a direction parallel to the apical dendrite (red and green arrows in *B* and *C*, respectively).

if and how beta events could be reproduced in our dipole model. We first investigated how the statistically significant features of the beta events within and across subjects, which occurred in the middle of the waveforms between PK1 and PK5 (Fig. 1 *B*, *i* and *SI Appendix*, Tables S1 and S2) could be explained in our model. We found that a beta event waveform consistent with all the statistically significant features of the human data could be reproduced by single bursts of nonrhythmic excitatory synaptic input to the cortical circuit that consisted of a broad proximal drive (~100 ms) that was disrupted by a stronger distal drive that lasted a beta period (~50 ms) (Fig. 4*A*). More specifically, "bursts" of exogenous spikes were simulated and activated excitatory (AMPA) synapses in distinct laminar profiles (Fig. 4). Histograms of the profile of driving spikes over 50 simulations are shown in Fig. 4*B*, *Upper*. In each simulation, the burst profile of the driving spike trains was stochastic, with a variance of 20 ms for the proximal drive and 15 ms for the distal drive and a 0-ms mean delay between the proximal and distal drive arrival times (i.e., the proximal and distal drives were nearly simultaneous) (*SI Appendix*, *Experimental Procedures*, *Computational Modeling*). This pattern of input reproduced each of the statistically significant features of the beta event waveforms observed in the human data (Fig. 4*B*, *Lower* and *SI Appendix*, Table S4). The PK2 and PK4 peaks were positive, and PK3 was negative. The magnitude of the PK3 trough was largest, and the transition to this trough was steeper than the transitions to the side troughs ($P < 0.01$) (*SI Appendix*, Table S4). The crucial factor defining the beta event frequency was the duration of the distal drive, which was simulated to last one beta period (~50 ms). The distal drive set the PK3 duration, which in turn was linearly correlated with the beta period (*SI Appendix*, Table S3; see also mean PK3 duration in *SI Appendix*, Table S4).

The beta event waveform in Fig. 4 resulted from a broad proximal drive that initially pushed the current flow up the PN dendrites to create the PK2 peak (left red arrow in Fig. 4*B*). This drive was disrupted by the faster and effectively stronger distal drive that pushed current flow down the PN dendrites to create the sharp PK3 trough that lasted a beta period (green arrow in Fig. 4*B*). When the distal drive ended, residual drive from the initial proximal input pushed current flow back up to create the PK4 peak (right red arrow in Fig. 4*B*). The current flow then relaxed back to zero. Importantly, as in our prior study (1), the strength of the exogenous drives was chosen to be subthreshold such that the waveform shape was set by the parameters of the drive and subthreshold dendritic dynamics and not by local spiking interactions.

Nearly simultaneous 10-Hz proximal and distal drives create additional waveform features and continuous oscillations. The results detailed above show that rhythmicity in the drives was not necessary to reproduce the significant features of the individual beta events, which were contained between PK1 and PK5 (Figs. 1*B* and 4). However, the rising endpoints of the oscillations and resultant PK1 and PK5 apparent in some trials, particularly in IFC, and apparent in the averaged beta event waveforms across subjects (Fig. 1 *B*, *ii* and *iv*, *Lower*) were missing in simulations consisting of single cycles of broad proximal and strong distal drives. These trends and other features of the continuous 1-s signals (Fig. 1*A*) could be reproduced when the proximal and distal drives were simulated to arrive nearly simultaneously at 10 Hz, as in our prior studies (Fig. 5*A*) (1, 33).

Fig. 5*C*, *Lower* shows the average of 50 high-power beta events pulled from 50 simulations with continuous, nearly synchronous 10-Hz proximal and distal drives over 1 s (e.g., Fig. 5*B*), where the SD of the proximal drive on each cycle was 20 ms and the SD of the distal drive was 5, 10, 15, or 20 ms (Fig. 5*C*, *Upper*). Fig. 5*D* details the case in which the distal drive SD was 15 ms, which strongly resembles that shown in Fig. 1 *B*, *i*. In each case, the rising endpoints of the oscillation and resultant PK1 and PK5 were induced by the prior and next cycle of the ongoing 10-Hz proximal drive that pushed the current flow back up the dendrites (red arrows in Fig. 5*D*). The PK1 and PK5 peaks became negative as the distal drive SD was increased with a corresponding decrease in the PK3 magnitude (blue curve in Fig. 5*D*; distal SD = 20 ms). This result suggests that the negative PK1 and PK5 troughs observed in the average IFC beta events could be created by a distal drive with a broader SD. Each simulation in Fig. 5*C* also reproduced the statistically significant features of the beta event waveforms (*SI Appendix*, Table S4).

Given this beta event mechanism, the duration and magnitude of the PK3 trough were controlled by the variance of spikes in each burst event arriving at the distal dendrites (Fig. 5 *E* and *F* and *SI Appendix*, Table S4). As the variance increased, the duration of the PK3 trough increased (Fig. 5*D*), and the amplitude decreased (Fig. 5*F*). Pooling the data across four SDs, we found that the duration of the PK3 trough was linearly correlated with the corresponding beta period for a given event and was a better predictor than the duration between the neighboring peaks, as is consistent with the human data (*SI Appendix*, Table S3).

The MEG data in Fig. 1*A* show that beta events in SI and in IFC can co-occur with or without a strong alpha signature. By changing the effective strength of the distal drive, the relative alpha to beta expression could be modulated in our model. When the SDs of the proximal and distal drives on each cycle of the input were similar, prominent alpha and beta oscillations

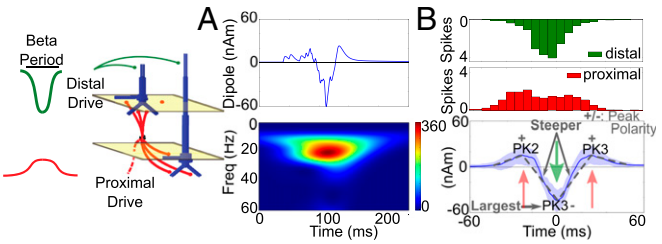

Fig. 4. Beta events were reproduced in a model with a broad proximal drive disrupted by a strong distal drive that lasted one beta period. (*A*) Example of a current source dipole waveform and spectrogram from a simulation in which the cortical network was driven by a broad burst of action potentials, eliciting excitatory postsynaptic currents in a proximal drive pattern and lasting ~100 ms simultaneous with a sharper, more synchronous burst of action potentials eliciting excitatory postsynaptic currents in a distal drive pattern lasting one beta period (~50 ms). Spectrogram units: $(Am)^2$. (*B*, *Upper*). Histogram of the spiking pattern of the drive over 50 such simulations. (*Lower*) Average (±SD) of 50 simulations showing a beta event waveform consistent with statistically significant features in the human data (*SI Appendix*, Table S3).

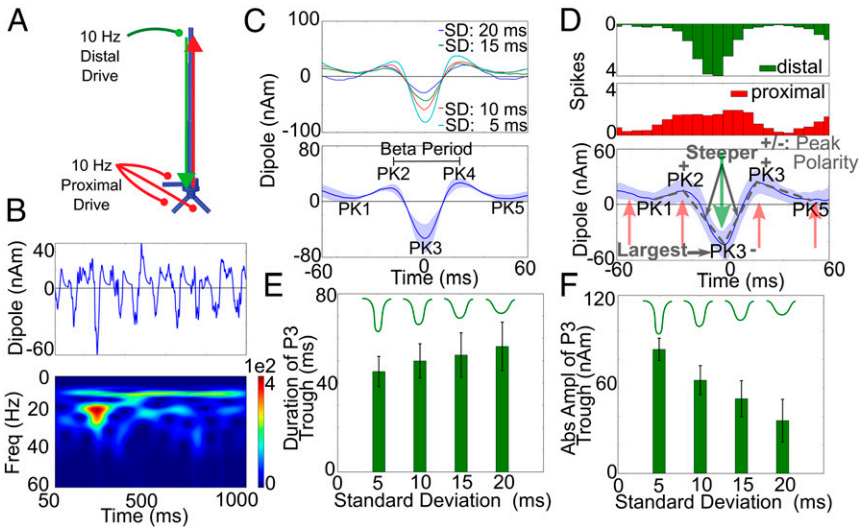

Fig. 5. Nearly simultaneous 10-Hz proximal and distal drives reproduced additional beta event waveform features, and PK3 was dependent on the distal drive. (*A*) Illustration with 10-Hz proximal and distal drives. (*B*) Example of a dipole time course and spectrogram over 1 s [distal SD, 15 ms; proximal SD, 20 ms; mean delay, 0 ms, units: $(AM)^2$] exhibiting high-power beta events. (*C*, *Upper*) Average current source waveform during 50 high-power beta events for each of four different SD of the distal drive burst. (*Lower*) Averaged data for the four different SD. (*D*) Histogram of driving spikes during 50 high-power beta events as in *B* (distal SD, 15 ms) and mean and SD of corresponding waveforms. Beta event waveforms consistent with the human data emerged (*SI Appendix*, Table S3), as did the PK1 and PK5 troughs and the rising endpoints of the beta event waveform observed in the average human data (Fig. 1*B*). (*E* and *F*) Duration and peak amplitude of the PK3 for the four SDs of distal drive.

both occurred, and on average alpha was dominant. When the distal SD was decreased relative to the proximal SD (e.g., distal SD = 5 ms, proximal SD = 20 ms), beta activity became more prominent (*SI Appendix*, Fig. S1; also see ref. 1). We have shown previously that, when the proximal and distal drives were not nearly simultaneous (as in Fig. 5), beta occurs less often, and in the case of antiphase drive (mean delay 50 ms) a pure alpha signal emerges (*SI Appendix*, Fig. S2*D*) (1).

As described above, rhythmicity of the inputs was not required to produce beta events. As long as proximal and distal inputs arrive at the neocortex nearly simultaneously and the distal drive is stronger and lasts ∼50 ms (Fig. 4), beta events with all of the statistically significant waveform features between the PK1 and PK5 peaks can emerge. In fact, when the proximal drive was simulated with a uniform random process and paired with strong ∼50-ms distal drive arriving at various slow frequencies, high-power beta events still emerged in our signal [10-Hz distal (*SI Appendix*, Fig. S2*A*) and 1-Hz distal (*SI Appendix*, Fig. S2*B*)]. In these simulations, beta events once again emerged when a broad, weak proximal drive lasting ∼100 ms occurred simultaneously with a distal drive that was stronger and lasted a beta period (∼50 ms). A similar phenomenon was observed when a broad proximal drive and a sharp distal drive were simulated simultaneously but infrequently (1-Hz proximal and distal, *SI Appendix*, Fig. S2*C*).

A 20-Hz drive does not account for beta events. A prevailing theory on the origin of neocortical beta in humans is that it originates in the basal ganglia (20, 21) and is propagated via thalamus to neocortex. The ventral–medial (VM) nucleus of the thalamus receives direct basal ganglia input and predominantly contacts supragranular layers broadly across the neocortex (40). We therefore investigated the impact of beta periodic drive to the distal apical dendrites of the PNs in our model (Fig. 6; also see *SI Appendix*, Fig. S3). This drive was produced by generating a sequence of bursts of action potentials to the distal dendrites of the PNs (Fig. 6*A*) with a mean interburst interval of 50 ms (20-Hz drive). The variance of the burst spike times on each cycle was chosen so that each burst lasted one beta period on average, as in the prior simulations (Fig. 6*C*, *Upper* and *SI Appendix*, Fig. S3).

As expected, the beta-frequency periodic drive produced beta rhythmicity in the current source signal (Fig. 6*B*). The network started in a resting state, and the excitatory synaptic drive from each burst event drove current flow down the apical dendrites (green arrows in Fig. 6*C*, *Lower*), which then relaxed back toward zero. The unidirectional flow of current along the PN dendrites produced a waveform exhibiting mostly negative polarity, in contrast to the human SI and IFC data that consistently oscillated around zero. Averaging 50 high-power beta events from this signal, as in the prior analysis, showed that the waveform also lacked the shape of the human data (Fig. 6*C*, *Lower*). The magnitude of the PK1 and PK5 troughs were statistically equivalent to the PK3 trough, and the steep slopes around the PK3 trough relative to the neighboring peak transitions were missing also ($P > 0.01$) (*SI Appendix*, Table S4).

These simulations assumed that the baseline current sources were at rest and that the 20-Hz distal VM drive was the only input to the network. An alternative, perhaps more realistic, assumption for in vivo recordings is that this thalamic drive occurs in conjunction with a thalamic drive to granular/infragranular layers. Evidence suggests that during spontaneous resting brain states such drive likely occurs at ∼10 Hz (41). We therefore paired the 20-Hz distal dendritic input with a simulated 10-Hz lemniscal excitatory synaptic drive that contacted proximal PN dendrites. This pairing also generated neocortical beta events (*SI Appendix*, Fig. S3). Alternating current flow was driven up and down the PN apical dendrites creating an oscillatory signal around zero. Once again, however, the beta event did not have the shape of the human data (*SI Appendix*, Table S4; see also *SI Appendix*, *Supplemental Discussion*). As predicted by this simulation, we did not find evidence of beta frequency distal drive in the laminar recordings from SI, as described below.

Intracortical beta generation from spike-mediated synaptic interactions and M-currents does not account for beta events. All the prior simulations consider exogenously driven patterns of activity in macroscopic current source signals, where the strength of the drive was titrated to create subthreshold current flow in the PN dendrites. In contrast, several prior studies have shown that the neocortex can generate beta rhythms locally from the spiking interactions of local cortical circuits. More specifically, prior in vitro experiments and models have established that networks of PNs and inhibitory neurons whose spiking is reciprocally coupled through fast excitation (AMPAergic) and inhibition (GABAergic) can produce beta rhythms, provided that the PNs contain a voltage-dependent M-type potassium current, which gates the rhythmic firing time of the cells to a beta period (22–25).

We simulated such an M-current–mediated beta rhythm in a reduced network of synaptically coupled PNs and inhibitory neurons and investigated the resulting current source signal in the network (Fig. 7). To simulate transient (<150 ms) beta oscillations in the spiking network, we drove the PNs, which contained M-currents, with a brief (150 ms) burst of noisy excitatory synaptic drive (Poisson spike rate; see *Experimental Procedures* and *SI Appendix*, Fig. S4*A* for an example with shorter-duration Poisson drive). This drive effectively turned on a transient bout of rhythmic spiking activity in the network over a 150-ms window. As in prior studies (22–25), the network parameters were

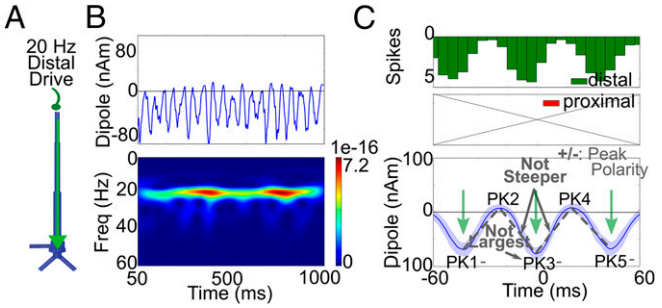

Fig. 6. 20-Hz rhythmic distal drive does not account for the beta event waveform. (*A*) Illustration of 20-Hz distal drive directly to supragranular layers. (*B*) Resulting 1-s current dipole waveform and spectrogram [units: $(AM)^2$]. (*C*) Histogram of driving spikes to the local network during high-power beta events extracted from 50 such simulations. The beta event waveforms did not have the same features as the human data (*SI Appendix*, Fig. S3 and Table S4).

tuned to a regime in which the population of PNs fired spikes at a beta frequency, creating a beta event in the current dipole signal (Fig. 7*B*). The beta event began with a small burst of action potentials in the PN that induced noisy current flow in the PN dendrites. The spiking activity in the PN recruited the local inhibitory interneurons, which in turn inhibited the PN from firing and created a small net downward deflection in dendritic current flow (PK1). Once the inhibition and M-current kinetic effects wore off, the PN fired a second burst of spikes, creating strong and fast back-propagating current flow up the apical PN dendrites (PK2), followed by a second bout of inhibition (PK3). Once the effect of the second bout of inhibition wore off, there was a third round of PN firing (PK4) followed by a strong repolarization of the dendrites (PK5).

In nonaveraged single simulations (Fig. 7*B*), the resultant current dipole signal was noisier than in the human data and in the prior simulations that relied on subthreshold current flow. The noise resulted from the noisy excitatory drive and from the PN action potentials creating a strong and fast back-propagating upward current flow in the apical dendrites followed by dendritic repolarization and a downward current flow (see also refs. 34 and 35). The average current dipole from 50 such transient activations shows a beta event waveform that lasted approximately three periods, as in the human data, albeit with a larger variance across trials (Fig. 7*C*). In this case, the PK3 duration was approximately one beta period, as in the human data (*SI Appendix*, Table S4). However, the PK3 trough was not the most prominent feature of the waveform and was not significantly different from zero. Further, the slopes around the PK3 were not the steepest slopes (*SI Appendix*, Table S4). Several tested parameter variations, including threefold increases in the strength of local inhibition and maximal M-current conductance or an increase in the rate of the Poisson input (*SI Appendix*, Fig. S4 *B–D*), did not reproduce the significant features of the human beta event waveforms. In each case, the PK3 trough never became the most prominent feature in the beta event.

Longer 1-s simulation with continuous Poisson drive to the PNs produced robust beta activity. The average of high-power beta events taken from 50 such simulations showed consistently positive and larger PK2 and PK4 peaks (Fig. 7 *D* and *E*). However, the significant features of the beta event waveform were still absent, even with parameter variations, as described above (*SI Appendix*, Fig. S4 *D* and *E* and Table S4).

Laminar LFP Recordings in Monkey and Mouse Support Model-Derived Predictions.

Beta event profiles are consistent in monkey and mouse LFP. To test our model-derived predictions on the origin of beta events directly, we investigated signatures of beta activity in laminar neocortical LFP and current source density (CSD) recordings in vivo from SI in monkeys and mice. Based on electromagnetic physics and neocortical anatomy, strong postsynaptic intracellular electrical current in the apical dendrites of synchronous populations of PNs would also produce ohmic return (volume) currents and associated potential distributions outside the cells that can be recorded as LFPs with microelectrodes (Fig. 2). Although LFPs depend heavily on the local conductivity gradients and the anatomy, physiology, and synchrony of the local networks, the synaptic currents on the spatially aligned and parallel-oriented neocortical PN dendrites are thought to dominate this signal (36, 42). Thus, if the postsynaptic primary currents are large enough (e.g., involve the participation of many PNs), the estimated current source and LFP from middle neocortical layers should be directly comparable. Assuming that subthreshold postsynaptic primary currents enter the PNs at one end of the apical dendrites and escape at the opposite end, the intracellular currents and the vertical gradient of the extracellular LFPs are in the same direction. The corresponding primary and volume currents flow in opposite directions (36, 43, 44). This assumption enables direct comparison between current source signals and LFPs (Fig. 8*A*).

We recorded spontaneous oscillations in the granular layer LFP in SI of anesthetized mice (vibrissa neocortex; $n = 3$ penetrations, 2 animals) and awake macaques during nontask conditions (hand area of SI; $n = 29$ penetrations, 3 animals) to investigate if spontaneous beta events in these signals had the same characteristic waveform features as the human SI beta events (Fig. 1). Robust beta events emerged as noncontinuous events in the LFP from the granular layers in both preparations. *SI Appendix*, Fig. S5*A* shows the definition of layers, and *SI Appendix*, Fig. S5 *C* and *D* shows examples of waveforms and spectrograms from spontaneous 1-s signal. Further, in each animal, the duration of the high-power beta events was <150 ms (*SI Appendix*, Table S5),

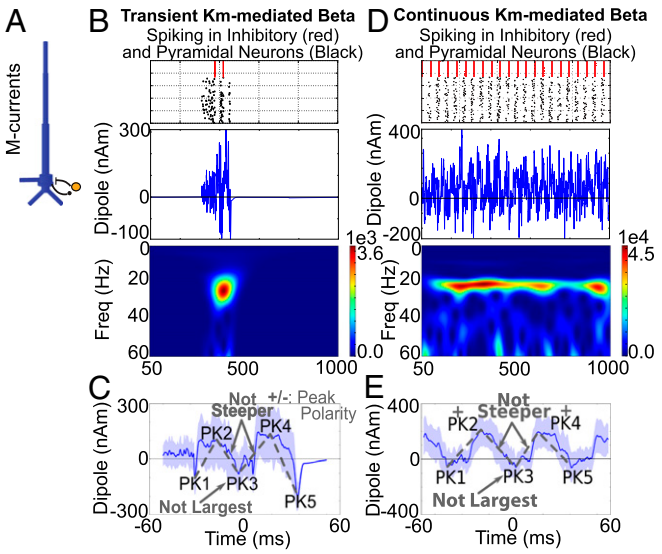

Fig. 7. M-current– and inhibition-mediated beta events in spiking networks do not account for beta event waveforms. (*A*) Illustration of network used to simulate spike-mediated beta oscillations. (*B*) Raster plot of induced transient spiking activity in PNs and inhibitory neurons during a brief (150 ms) bout of random excitation to the local network, with resultant dipole waveform and spectrogram [units: $(Am)^2$]. (*C*) Average and SD of corresponding current source signal from 50 such transient simulations aligned in time showing that transient beta events lasted approximately three periods. In this case, the shape of the waveform did not match the human data (*SI Appendix*, Table S4). (*D*) Continuous excitation to the network over a 1-s simulation induced repeated bouts of beta activity. (*Top*) Spiking raster plot. (*Middle*) Dipole. (*Bottom*) Spectrogram. (*E*) Average of 50 high-power beta events extracted from the continuous-drive simulations. The waveform was not consistent with the human data (see *SI Appendix*, Fig. S4 for variations in parameters).

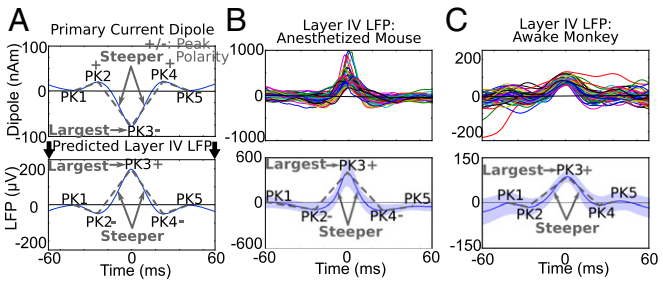

Fig. 8. Beta events in granular layer SI LFP from an anesthetized mouse and an awake monkey had waveform features consistent with the human data. (*A*, *Upper*) Schematic reproduction of the mean primary current dipole and statistically significant features of the beta event waveform. (*Lower*) Predicted beta events in the LFP from granular layers, if the current dipole and layer IV LFP events are generated by the same underlying mechanisms, e.g., currents flowing within the deep-layer PN dendrites (Fig. 2). (*B*, *Upper*). Examples of 50 unfiltered high-power beta events from layer IV of SI (vibrissa neocortex) in an anesthetized mouse. (*Lower*) Mean and SD defined and aligned as in the human data. (*C*) As in *B*, showing data from layer IV of area 3b in an awake monkey during spontaneous periods. The granular layer beta event waveform from each animal was consistent with the human data (*SI Appendix*, Table S5; also see *SI Appendix*, Fig. S5*A* for definition of layers).

as in the human data. The shape of averaged high-power LFP beta events resembled an inversion of the human data, as expected if the underlying mechanisms of induction were the same and were dominated by large PNs (Fig. 8 *B* and *C*). We tested if the shape of these beta events matched the statistically robust features of SI human current source data and found that each feature was consistent ($P < 0.001$) (*SI Appendix*, Table S5). In each animal, the duration of the PK3 trough was within the beta period.

Model accurately predicts the beta event CSD. The close agreement between the human current source and animal LFP data suggested that the temporal signature of high-power beta events was conserved across recording modalities, supporting the idea that they were created by the same underlying neural mechanisms. To test directly the model-derived prediction that these beta events emerged from a specific pattern of exogenous excitatory synaptic drive to the local neocortical circuit, we next applied CSD analysis to our laminar LFP data. Excitatory synaptic events are known to create depolarizing current flow across the cell membrane, reflected as a negative sink in a CSD profile (42, 45). These synaptic depolarizations coincide with opposing transmembrane currents, reflected as a positive source, at a distance from the synaptic event where the current can escape the cell membrane, creating sink/source pairings (Fig. 2).

Our model predicted that beta events were induced by precisely timed excitatory synaptic events to the PN dendrites in distinct layers (Fig. 9*A*). The predicted CSD pattern evoked by this sequence of drive would be dominated by a strong sink in the location of the PN distal dendrites in the supragranular layers lasting approximately a beta period. Simultaneous with the supragranular sink, we predicted weaker and broader sinks in locations near the supra- and infragranular layer PN proximal dendrites (Fig. 9*B*).

The model-derived predictions were confirmed in the CSD data (Fig. 9 *C* and *D*). The dominant activity was a sink in the supragranular layers during a beta event (green boxes) whose duration was within the beta period for both datasets [monkey: $n = 29$ penetrations, mean ± SE = 47 ± 3 ms (Fig. 9 *D* and *F*); anesthetized mouse: $n = 3$ penetrations; mean ± SE = 37 ± 18 ms (Fig. 9*C*)]. Weaker and broader sinks were observed simultaneously near the location of the proximal dendrites between the granular and supragranular layers and in the infragranular layers. Comparison of the maximum amplitude of the sink activities confirmed that on average the amplitude of the supragranular sink was greater than the amplitude of the sink in the infragranular layer in each animal [monkey (Fig. 9*E*): $P < 0.005$, *t* test; supra: mean ± SE = 11.37 ± 2.13 μV/mm^2; infra: mean ± SE = 4.56 ± 0.59 μV/mm^2; mouse: $n = 3$ penetrations too low for statistical analysis; supra: mean ± SE = 0.0084 ± 0.0038 μV/mm^2; infra: mean ± SE = 0.0057 ± 0.0012 μV/mm^2).

Our model results predicted that the duration and amplitude of the distal synaptic event determined the duration and amplitude of the granular layer LFP PK3 peak (Fig. 5 *E* and *F*). To test this prediction, we correlated the duration and amplitude of the supragranular sink with the duration and amplitude of the PK3 peak in the monkey LFP data. Fig. 9 *F* and *G* show that both features were significantly correlated ($P < 0.05$), and the duration of the PK3 peak was in the beta period (*SI Appendix*, Table S5; see *SI Appendix*, Fig. S5*B* for beta waveforms in other layers).

Discussion

Building on prior work (1, 15, 33), we present converging evidence supporting a new theory regarding the mechanistic origin of spontaneous neocortical beta oscillations. We show that nonaveraged spontaneous beta activity in SI and frontal cortex emerges as brief events that typically last <150 ms (1, 30). These beta events co-occur with varying levels of alpha activity, depending on the subject and area studied. Quantification of the temporal profile of the unfiltered high-power beta event waveforms reveals a stereotypical pattern that is conserved across humans, monkeys, and mice, where the frequency is set by a dominant peak in the event waveform that lasts approximately one beta period. To our knowledge, this analysis is the first time beta event waveforms have been examined and quantified in the temporal domain, revealing tangible markers against which computational model predictions can be tested and from which our theory developed. Our modeling suggested that individual beta events do not necessarily depend on rhythmic inputs. Rather, the statistically robust features of individual high-power beta events in nonaveraged data (constrained between PK1 and PK5) depend exclusively on the relative timing and strength of synchronous proximal and distal drives. A single cycle of broad proximal drive (~100 ms) that was disrupted by a simultaneous stronger and shorter distal drive that lasted a beta period (~50 ms) was sufficient to create such a beta event. Continuous 10-Hz rhythmicity of the driving inputs produced additional features of the longer-duration rhythmic activity (e.g., 1 s), which was dominated by alpha or beta depending on the strength and duration of the distal drive. We show that these model-derived predictions account for distinct features of MEG measured beta events, whereas several other possible beta mechanisms do not. Laminar LFP and CSD recordings in SI of both anesthetized mice and awake monkeys further support the model-derived predictions. The agreement among human, model, and animal data suggests that this mechanism for spontaneous in vivo neocortical beta events is conserved across brain areas, species, and recording modalities.

Relation to Other Established Models of Beta Generation. The mechanism of beta generation proposed here was able to account for beta events observed in vivo in spontaneous SI and IFC oscillations from human current source signals. These so-called "macroscopic" signals are assumed to come from the subthreshold dendritic currents in large populations of synchronous and spatially aligned neocortical PNs (36–38, 43), which are continuously influenced by synaptic drives from other brain areas. This assumption is consistent with studies showing that low-frequency rhythms correspond with decreased multiunit activity in vivo (9, 46). Our model reproduced such events from synaptically driven subthreshold activity in multi-compartment PN dendrites. This beta mechanism would not have been discovered in a model that simulated a reduced representation of neural activity, e.g., single-compartment neurons. Support for this mechanism also was observed at the mesoscopic scale from extracellular laminar LFP recordings in SI in anesthetized mice and in awake monkeys during spontaneous nontask periods, suggesting that

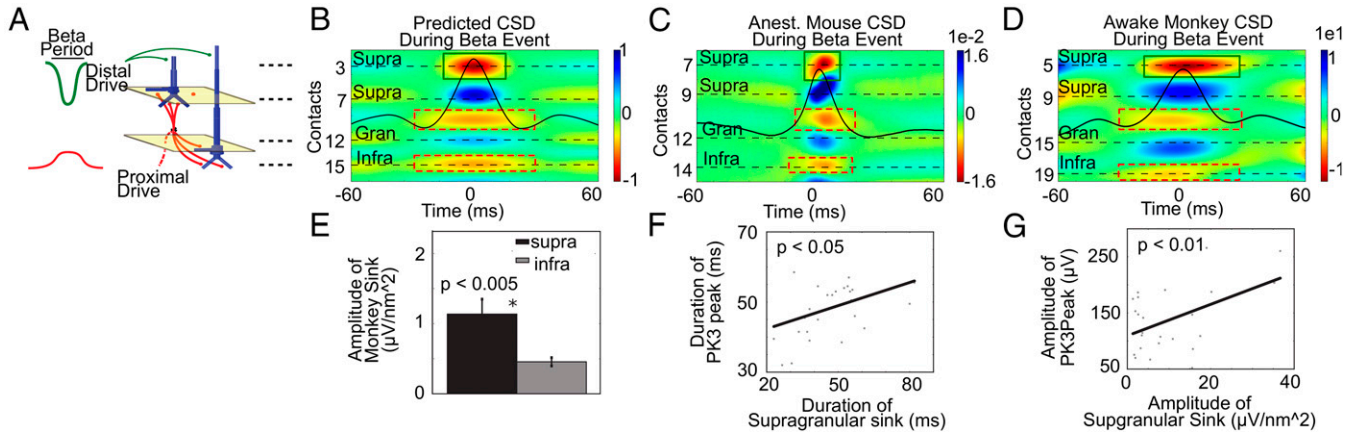

Fig. 9. CSD analysis showed patterns of synaptic excitation during beta events in an anesthetized mouse and an awake monkey as predicted by the model. (*A*) Illustration of the simultaneous proximal and distal excitatory synaptic drives inducing beta events as predicted by our model. (*B*) Corresponding predicted CSD pattern with overlaid layer IV beta event waveform. (*C* and *D*) The sink/source pairings in the animal data were consistent with the model predictions, as outlined schematically with green and red boxes. Examples of the CSD pattern from SI laminar recordings in an anesthetized mouse (*C*) and an awake monkey (*D*) during high-powered beta events in layer IV aligned to the maximal peak of the beta event (mean $n = 50$ events; beta event is overlaid). (*E*) In the monkey data, the amplitude of the supragranular sink was statistically larger than that of the infragranular sink ($P < 0.005$). (*F* and *G*) The supragranular sink duration (*F*) was within the beta period and linearly correlated with the duration of the PK3 peak (Pearson's correlation $P < 0.05$), as was the amplitude ($P < 0.01$) (*G*).

this mechanism is generalizable to spontaneous SI beta events at smaller spatial scales in vivo. This mechanism may not account for beta at different recording scales or behavioral states [e.g., motor hold conditions (27, 28) or up-states (47)] or in other brain networks, particularly those without spatially aligned PNs such as inhibitory networks in the striatum, where other mechanisms have been proposed (21).

Prior modeling and experiments, primarily from slice recordings, have established that neocortical beta rhythms can emerge from the spiking interactions of local excitatory and inhibitory populations (22–26). Beta in the LFP of slice preparations, including those from somatosensory (22) and motor neocortex (24), operates in a similar 20- to 30-Hz range, dominated by the activity of layer V PNs. In these prior studies, beta was explicitly dependent on spiking interactions among local neurons, without the necessity of external synaptic drive.

A key factor in beta generation in these prior studies was the recruitment of the M-type potassium current in the excitatory PNs. The M-current belongs to a class of post-hyperpolarization potassium currents that create adaptation during repetitive spiking, and the beta frequency is critically dependent on the suprathreshold activation of the M-current that sets the firing time of the PNs in mutually coupled excitatory and inhibitory networks (e.g., Fig. 7) (22–26). The PNs in our model included M-currents and other active currents. However, at subthreshold activation levels these currents do not influence the dendritic current flow; instead, the flow is determined by the time constants and strength of synaptic activation and the cable properties of the dendrites. Furthermore, although the prior models suggest that beta rhythms reflect repeated bouts of spiking activity separated by a beta period, our model suggests that beta can reflect a single bout of activity that lasts a beta period. Thus, the beta generation in human signals presented here is qualitatively different from prior models.

Within the large population of subthreshold-driven PNs in the human signal, there is likely a smaller subpopulation of neurons firing action potentials, potentially in phase with the driven currents (7). This prediction is not currently represented in our model. Based on estimates on the size of current dipole signals produced by spiking activity in individual PNs (34, 35, 37), spiking activity in a small population of neurons would not impact our results provided the spiking is sufficiently sparse and desynchronized relative to the size of the network producing the subthreshold oscillation.

Relation to Beta in Other Neocortical Areas and Thalamic Nuclei. The beta theory proposed here is relevant to in vivo macroscopic- and mesoscopic-scale recordings of spontaneous beta events presumed to emerge from the synchronous activity in large populations of PNs. The model construction was based on generalizable features of neocortical circuitry and accounted for the dominant features of spontaneous non–stimulus-locked beta events in primary sensory and frontal cortex. An important open question is whether our model can account for spontaneous beta events in other neocortical areas, e.g., motor cortex, or if it can account for stimulus-locked sensory- or motor-evoked beta signals. The essential anatomical feature underlying this mechanism is the existence of distinct laminar-specific excitatory synaptic drives to distal and proximal dendrites of spatially aligned PN dendrites. This architecture is supported across the neocortex, where distinct thalamic nuclei could provide the laminar-specific drive (48, 49), or could be a combination of thalamocortical and cortical–cortical inputs. The sources of drive could change depending on the behavioral state and areas studied.

We conjecture that in the spontaneous state studied here the proximal and distal synaptic drives creating beta events likely arise from separate thalamic nuclei. In primates two functionally and neurochemically distinct pathways link thalamus with neocortex: (*i*) a focally projecting, so-called "driving" pathway that carries sensory information from the periphery or motor commands from subcortical structures to granular and infragranular cortical layers, and (*ii*) a widespread, nonspecific modulatory pathway projecting directly to the supragranular layers (48, 49). The distal-projecting pathway has been shown to modulate the overall activity of the recipient area without necessarily eliciting spikes, as required in our model (50, 51).

Several lines of inference indicate that these parallel thalamic pathways may provide the proximal and distal drives in our model. A recent study of simultaneous thalamic and neocortical activity in humans shows coupling of alpha activity in the thalamus to beta in the neocortex (52). Among the nonspecific thalamic nuclei, the VM/pallidal thalamus is known to project dominantly and diffusely to the supragranular layers in sensory and motor cortex (40) as well as prefrontal cortex (40, 53, 54), making it particularly well suited for the distal drive in our model. VM as a source of the distal drive would also provide a direct connection between our theory and the origin of beta disruption in PD (*SI Appendix*, *Supplemental Discussion*). Other thalamic nuclei have targets in proximal and distal locations, such as the posterior medial nucleus (POm) to somatosensory

cortex (55), which could be a single source of both drives. In motor cortex, two distinct thalamocortical projection pathways to primary motor cortex in proximal and distal projection patterns have been shown to emerge from distinct thalamic zones (55, 56).

The model prediction that two stochastic 10-Hz drives can produce beta events emerging as part of more continuous rhythms with variable levels of alpha activity is supported by the known propensity of thalamic nuclei to fire bursts of activity at alpha frequencies during spontaneous states (41, 57, 58). Importantly, the thalamic bursts have been shown with whole-cell recordings to have a duration of ∼50 ms (51), in direct agreement with our model prediction.

The thalamus is also well poised to coordinate the synchronized proximal and distal drives as required by our theory. Synchronized alpha activity has been observed across thalamic nuclei, likely mediated by widespread inhibitory drive from the reticular nucleus. Furthermore, although there is evidence that thalamic nuclei express beta in LFP signals (47), the precise biophysical origin of LFP in thalamus is poorly understood. Thalamic beta could readily reflect cortically driven activity or single bursting events that last ∼50 ms (45), as required by our model. Thalamic bursts lasting ∼50 ms also could be imposed by bursting activity in basal ganglia, as has been observed in PD pathophysiology (59).

Last, we note that the distal drive in our model reflected a burst of action potentials activating fast AMPA synapses. We postulate that a similar effect may be achieved by fewer spikes activating slower receptors, provided the net synaptic effect lasts a beta period. Finer-scale details and possible sources of exogenous drive need to be tested further with invasive recordings.

Beta Expression in Neocortex Inhibits Processing via Decreased Top-Down Communication through Supragranular Channels. Beta expression and its coherence between distinct brain foci are thought to contribute to information processing at several levels, including communication between neocortical areas (3, 8, 12), the protection of current behavioral and processing states from interruption (11), and memory maintenance. Our results provide a unifying link between studies suggesting that beta coordination mediates top-down neocortical processing (11, 12, 60) and studies showing that top-down influences are communicated through supragranular layers (61), because the described beta mechanism is explicitly dependent on strong excitatory synaptic drive to supragranular layers. A key unifying theme for sensorimotor beta expression is its negative correlation with active processing (7, 11, 18). Sensorimotor beta shows an inverse relationship with attention (2, 14, 15, 29), sensory detection probability (2), accurate decision-making (62), and movement planning and initiation (6). Together, these results suggest that beta rhythms inhibit processing and decrease focally to allow optimal information relay.

Our results lead to three specific predicted mechanisms by which neocortical beta events would decrease information relay. The first is direct recruitment of inhibition in the supragranular layers. Although the model and CSD results suggest that the net impact of this strong, ∼50-ms supragranular synaptic drive inducing beta is excitatory in nature, producing a sink and subthreshold dendritic currents down the PN, this drive likely also synapses on the supragranular inhibitory neurons, increasing the prestimulus inhibitory tone. A class of somatostatin-positive interneurons that synapse on the distal dendrites of PNs has been suggested to be optimally driven by an alpha-frequency rhythmic drive, making them particularly well suited to mediate such inhibition according to our model (63). An increase in inhibition in the supragranular layers would diminish any subsequent relay of top-down cortical–cortical information processing through supragranular channels (1, 2), potentially in a phase-dependent manner (7). A second potential avenue of diminished information relay is saturation of the excitatory receptors on the PN distal dendrites; such saturation could similarly decrease the efficacy of top-down communication through supragranular channels. Assuming thalamic nuclei provide the predicted drives, a third potential avenue for diminished information relay is decreased relay of bottom-up sensory or motor information through the thalamus during high thalamic alpha states corresponding to the neocortical beta states in our model. Several mechanisms can account for impoverished sensory relay during alpha, including thalamic hyperpolarization, synaptic depression at thalamocortical synapses, and more generally the low capacity for novel external information relay during the co-occurrence of strong internally generated rhythms (64). Of note, none of these mechanisms suggests that beta needs to reflect repeated cycles of activity to impact function. Rather, our results suggest that local beta expression in these signals is the reflection of specifically timed synaptic events to distinct cortical layers and that these events, which occur intermittently in time, mediate beta's impact on behavior.

In conclusion, our theory of the origin of spontaneous beta events is supported across neocortical areas, recording modalities, and mammalian species. Our results lead to several testable predictions on the cellular level avenues by which beta emerges and may inhibit information processing and can guide future studies aimed at optimizing beta when it is disrupted in disease.

Experimental Procedures

The experimental procedures for each preparation and methodology have been published in prior work. We briefly outline key aspects and detail previously unreported analysis procedures. Additional details are available in *SI Appendix*.

MEG Data. The SI and IFC data were obtained in two prior studies (1, 15). A description of data collection and analysis in each study is presented in *SI Appendix, MEG Data Collection*. All MEG experimental protocols were approved by the Massachusetts General Hospital Internal Review Board, and each subject gave informed consent before data acquisition.

Computational Neural Model. The SI model was described previously (1), and the original code is available on the NEURON ModelDB website (https://senselab.med.yale.edu/modeldb/). See Fig. 3 and *SI Appendix, Computational Neural Modeling* for details.

Extracellular Laminar Recordings in Anesthetized Mice. LFP laminar data were obtained across the SI vibrissa barrel cortex in two neurologically healthy, anesthetized mice (one recording session for mouse 1; two recording sessions for mouse 2). A recording session is characterized by a new penetration of SI with the laminar probe. The probe was lowered to 1,600 μm into SI. Response to vibrissa deflections was used to confirm placement. Baseline activity was recorded for 10 min before a stimulus period consisting of 500 vibrissa deflections. For the purpose of this study, high-power beta events (Figs. 8 and 9) were analyzed only in the 10-min baseline period. Mice were housed and handled in accordance with Brown University Institutional Animal Care and Use Committee guidelines. The surgical and recording methods were as described previously (65); key features of data collection are detailed in *SI Appendix, Animal Data*.

Extracellular Laminar Recordings in Awake Monkeys. LFP laminar data were obtained in SI area 3b of three neurologically healthy, awake female rhesus macaques (*Macaca mulatta*) during 13, 4, and 12 recording sessions, respectively (*SI Appendix*, Table S5) using linear array multi-electrodes (Neurotrack, Budapest). Each recording session consisted of recordings of spontaneous neural activity (average length 4 min) and stimulation of the contralateral median nerve (mean of 140 stimuli per session). Here, beta events were analyzed only in the spontaneous recordings. Median nerve stimulation data were used to identify the neocortical layers. All experimentation was reviewed, approved, and monitored by the Animal Care and Use Committee at the Nathan Kline Institute and complied with United States Public Health Service guidelines for animal research. All surgical and recordings techniques were described previously (66); additional details are available in *SI Appendix, Animal Data*.

ACKNOWLEDGMENTS. We thank the editor and anonymous reviewers for thoughtful input; Charles Schroeder for generously providing the monkey data; and Hyeyoung Shin for help in analysis of mouse data and input on the manuscript. This work was supported by National Science Foundation Grant CRCNS-1131850 and NIH Grants R01 MH106174, 5T32MH019118-23, R01 MH060358, P41EB015896, and R01 EB009048.

1. Jones SR, et al. (2009) Quantitative analysis and biophysically realistic neural modeling of the MEG mu rhythm: Rhythmogenesis and modulation of sensory-evoked responses. *J Neurophysiol* 102(6):3554–3572.
2. Jones SR, et al. (2010) Cued spatial attention drives functionally relevant modulation of the mu rhythm in primary somatosensory cortex. *J Neurosci* 30(41):13760–13765.
3. Siegel M, Donner TH, Oostenveld R, Fries P, Engel AK (2008) Neuronal synchronization along the dorsal visual pathway reflects the focus of spatial attention. *Neuron* 60(4): 709–719.
4. Parkkonen E, Laaksonen K, Piitulainen H, Parkkonen L, Forss N (2015) Modulation of the ~20-Hz motor-cortex rhythm to passive movement and tactile stimulation. *Brain Behav* 5(5):e00328.
5. Buzsaki G (2006) *Rythms of the Brain* (Oxford Univ Press, New York).
6. Neuper C, Pfurtscheller G (2001) Event-related dynamics of cortical rhythms: Frequency-specific features and functional correlates. *Int J Psychophysiol* 43(1):41–58.
7. Miller KJ, et al. (2012) Human motor cortical activity is selectively phase-entrained on underlying rhythms. *PLOS Comput Biol* 8(9):e1002655.
8. Buschman TJ, Miller EK (2007) Top-down versus bottom-up control of attention in the prefrontal and posterior parietal cortices. *Science* 315(5820):1860–1862.
9. Haegens S, et al. (2011) Beta oscillations in the monkey sensorimotor network reflect somatosensory decision making. *Proc Natl Acad Sci USA* 108(26):10708–10713.
10. Buzsáki G, Logothetis N, Singer W (2013) Scaling brain size, keeping timing: Evolutionary preservation of brain rhythms. *Neuron* 80(3):751–764.
11. Engel AK, Fries P (2010) Beta-band oscillations–signalling the status quo? *Curr Opin Neurobiol* 20(2):156–165.
12. Bressler SL, Richter CG (2015) Interareal oscillatory synchronization in top-down neocortical processing. *Curr Opin Neurobiol* 31:62–66.
13. van Ede F, de Lange F, Jensen O, Maris E (2011) Orienting attention to an upcoming tactile event involves a spatially and temporally specific modulation of sensorimotor alpha- and beta-band oscillations. *J Neurosci* 31(6):2016–2024.
14. Bauer M, Oostenveld R, Peeters M, Fries P (2006) Tactile spatial attention enhances gamma-band activity in somatosensory cortex and reduces low-frequency activity in parieto-occipital areas. *J Neurosci* 26(2):490–501.
15. Sacchet MD, et al. (2015) Attention drives synchronization of alpha and beta rhythms between right inferior frontal and primary sensory neocortex. *J Neurosci* 35(5): 2074–2082.
16. Little S, Brown P (2014) The functional role of beta oscillations in Parkinson's disease. *Parkinsonism Relat Disord* 20(Suppl 1):S44–S48.
17. Heinrichs-Graham E, et al. (2014) Hypersynchrony despite pathologically reduced beta oscillations in patients with Parkinson's disease: A pharmaco-magnetoencephalography study. *J Neurophysiol* 112(7):1739–1747.
18. Leventhal DK, et al. (2012) Basal ganglia beta oscillations accompany cue utilization. *Neuron* 73(3):523–536.
19. Bevan MD, Magill PJ, Terman D, Bolam JP, Wilson CJ (2002) Move to the rhythm: Oscillations in the subthalamic nucleus-external globus pallidus network. *Trends Neurosci* 25(10):525–531.
20. Holgado AJ, Terry JR, Bogacz R (2010) Conditions for the generation of beta oscillations in the subthalamic nucleus-globus pallidus network. *J Neurosci* 30(37): 12340–12352.
21. McCarthy MM, et al. (2011) Striatal origin of the pathologic beta oscillations in Parkinson's disease. *Proc Natl Acad Sci USA* 108(28):11620–11625.
22. Roopun AK, et al. (2006) A beta2-frequency (20-30 Hz) oscillation in nonsynaptic networks of somatosensory cortex. *Proc Natl Acad Sci USA* 103(42):15646–15650.
23. Kramer MA, et al. (2008) Rhythm generation through period concatenation in rat somatosensory cortex. *PLOS Comput Biol* 4(9):e1000169.
24. Yamawaki N, Stanford IM, Hall SD, Woodhall GL (2008) Pharmacologically induced and stimulus evoked rhythmic neuronal oscillatory activity in the primary motor cortex in vitro. *Neuroscience* 151(2):386–395.
25. Jensen O, et al. (2005) On the human sensorimotor-cortex beta rhythm: Sources and modeling. *Neuroimage* 26(2):347–355.
26. Lee JH, Whittington MA, Kopell NJ (2013) Top-down beta rhythms support selective attention via interlaminar interaction: A model. *PLOS Comput Biol* 9(8):e1003164.
27. Baker SN, Olivier E, Lemon RN (1997) Coherent oscillations in monkey motor cortex and hand muscle EMG show task-dependent modulation. *J Physiol* 501(Pt 1):225–241.
28. Murthy VN, Fetz EE (1992) Coherent 25- to 35-Hz oscillations in the sensorimotor cortex of awake behaving monkeys. *Proc Natl Acad Sci USA* 89(12):5670–5674.
29. van Ede F, Köster M, Maris E (2012) Beyond establishing involvement: Quantifying the contribution of anticipatory α- and β-band suppression to perceptual improvement with attention. *J Neurophysiol* 108(9):2352–2362.
30. Feingold J, Gibson DJ, DePasquale B, Graybiel AM (2015) Bursts of beta oscillation differentiate postperformance activity in the striatum and motor cortex of monkeys performing movement tasks. *Proc Natl Acad Sci USA* 112(44):13687–13692.
31. Tan H, Jenkinson N, Brown P (2014) Dynamic neural correlates of motor error monitoring and adaptation during trial-to-trial learning. *J Neurosci* 34(16):5678–5688.
32. Lundqvist M, et al. (2016) Gamma and Beta Bursts Underlie Working Memory. *Neuron* 90(1):152–164.
33. Ziegler DA, et al. (2010) Transformations in oscillatory activity and evoked responses in primary somatosensory cortex in middle age: A combined computational neural modeling and MEG study. *Neuroimage* 52(3):897–912.
34. Jones SR, Pritchett DL, Stufflebeam SM, Hämäläinen M, Moore CI (2007) Neural correlates of tactile detection: A combined magnetoencephalography and biophysically based computational modeling study. *J Neurosci* 27(40):10751–10764.
35. Lee S, Jones SR (2013) Distinguishing mechanisms of gamma frequency oscillations in human current source signals using a computational model of a laminar neocortical network. *Front Hum Neurosci* 7:869.
36. Jones SR (2015) Local field potential, relationship to electroencephalogram (EEG) and magnetoencephalogram (MEG). *Encyclopedia of Computational Neuroscience Springer Reference*, ed Jaeger D Jr (Springer, Berlin).
37. Murakami S, Okada Y (2006) Contributions of principal neocortical neurons to magnetoencephalography and electroencephalography signals. *J Physiol* 575(Pt 3): 925–936.
38. Hamalainen M, Hari R, Ilmoniemi RJ, Knuutila J, Lounasmaa OV (1993) Magnetoencephalography - theory, instrumentation, and applications to noninvasive studies of the working human brain. *Rev Mod Phys* 65(2):413–497.
39. Okada YC, Wu J, Kyuhou S (1997) Genesis of MEG signals in a mammalian CNS structure. *Electroencephalogr Clin Neurophysiol* 103(4):474–485.
40. Herkenham M (1980) Laminar organization of thalamic projections to the rat neocortex. *Science* 207(4430):532–535.
41. Hughes SW, Crunelli V (2005) Thalamic mechanisms of EEG alpha rhythms and their pathological implications. *Neuroscientist* 11(4):357–372.
42. Buzsáki G, Anastassiou CA, Koch C (2012) The origin of extracellular fields and currents–EEG, ECoG, LFP and spikes. *Nat Rev Neurosci* 13(6):407–420.
43. Zhu Z, et al. (2009) The relationship between magnetic and electrophysiological responses to complex tactile stimuli. *BMC Neurosci* 10:4.
44. Ikeda H, Wang Y, Okada YC (2005) Origins of the somatic N20 and high-frequency oscillations evoked by trigeminal stimulation in the piglets. *Clin Neurophysiol* 116(4): 827–841.
45. Mitzdorf U (1985) Current source-density method and application in cat cerebral cortex: Investigation of evoked potentials and EEG phenomena. *Physiol Rev* 65(1): 37–100.
46. van Kerkoerle T, et al. (2014) Alpha and gamma oscillations characterize feedback and feedforward processing in monkey visual cortex. *Proc Natl Acad Sci USA* 111(40): 14332–14341.
47. Kuki T, et al. (2015) Contribution of parvalbumin and somatostatin-expressing GABAergic neurons to slow oscillations and the balance in beta-gamma oscillations across cortical layers. *Front Neural Circuits* 9:6.
48. Jones EG (2001) The thalamic matrix and thalamocortical synchrony. *Trends Neurosci* 24(10):595–601.
49. Barbas H, García-Cabezas MA, Zikopoulos B (2013) Frontal-thalamic circuits associated with language. *Brain Lang* 126(1):49–61.
50. Reichova I, Sherman SM (2004) Somatosensory corticothalamic projections: Distinguishing drivers from modulators. *J Neurophysiol* 92(4):2185–2197.
51. Sherman SM (2005) Thalamic relays and cortical functioning. *Prog Brain Res* 149: 107–126.
52. Fitzgerald TH, Valentin A, Selway R, Richardson MP (2013) Cross-frequency coupling within and between the human thalamus and neocortex. *Front Hum Neurosci* 7:84.
53. Jiménez-Castellanos J, Jr, Reinoso-Suárez F (1985) Topographical organization of the afferent connections of the principal ventromedial thalamic nucleus in the cat. *J Comp Neurol* 236(3):297–314.
54. Kolb B (1984) Functions of the frontal cortex of the rat: A comparative review. *Brain Res* 320(1):65–98.
55. Hooks BM, et al. (2013) Organization of cortical and thalamic input to pyramidal neurons in mouse motor cortex. *J Neurosci* 33(2):748–760.
56. Kuramoto E, et al. (2009) Two types of thalamocortical projections from the motor thalamic nuclei of the rat: A single neuron-tracing study using viral vectors. *Cereb Cortex* 19(9):2065–2077.
57. Contreras D, Steriade M (1995) Cellular basis of EEG slow rhythms: A study of dynamic corticothalamic relationships. *J Neurosci* 15(1 Pt 2):604–622.
58. Edgerton JR, Jaeger D (2014) Optogenetic activation of nigral inhibitory inputs to motor thalamus in the mouse reveals classic inhibition with little potential for rebound activation. *Front Cell Neurosci* 8:36.
59. Wichmann T, Dostrovsky JO (2011) Pathological basal ganglia activity in movement disorders. *Neuroscience* 198:232–244.
60. Womelsdorf T, Ardid S, Everling S, Valiante TA (2014) Burst firing synchronizes prefrontal and anterior cingulate cortex during attentional control. *Curr Biol* 24(22): 2613–2621.
61. Rockland KS, Pandya DN (1979) Laminar origins and terminations of cortical connections of the occipital lobe in the rhesus monkey. *Brain Res* 179(1):3–20.
62. Haegens S, et al. (2014) Thalamocortical rhythms during a vibrotactile detection task. *Proc Natl Acad Sci USA* 111(17):E1797–E1805.
63. Vierling-Claassen D, Cardin JA, Moore CI, Jones SR (2010) Computational modeling of distinct neocortical oscillations driven by cell-type selective optogenetic drive: Separable resonant circuits controlled by low-threshold spiking and fast-spiking interneurons. *Front Hum Neurosci* 4(4):198.
64. Klimesch W (2012) α-band oscillations, attention, and controlled access to stored information. *Trends Cogn Sci* 16(12):606–617.
65. Normand EA, et al. (2013) Temporal and mosaic Tsc1 deletion in the developing thalamus disrupts thalamocortical circuitry, neural function, and behavior. *Neuron* 78(5):895–909.
66. Lipton ML, et al. (2010) Interactions within the hand representation in primary somatosensory cortex of primates. *J Neurosci* 30(47):15895–15903.